Large tunnel magnetoresistance ratio in Fe/O/NaCl/O/Fe

Kui Gong,[1,2] Lei Zhang,[2,a)] Lei Liu,[3] Yu Zhu,[3] Guanghua Yu,[1] Peter Grutter,[2] and Hong Guo[2]
[1]*School of Materials Science and Engineering, University of Science and Technology Beijing, Beijing 100083, China*
[2]*Department of Physics, McGill University, Montreal, Quebec H3A 2T8, Canada*
[3]*Nanoacademic Technologies, Inc., Suite 320, 7005 Blvd. Taschereau, Brossard, Quebec J4Z 1A7, Canada*

(Received 15 June 2015; accepted 19 August 2015; published online 2 September 2015)

Magnetic tunnel junction (MTJ) is an important device element for many practical spintronic systems. In this paper, we propose and theoretically investigate a very attractive MTJ Fe(001)/O/NaCl(001)/O/Fe(001) as a two-terminal transport junction. By density functional theory total energy methods, we establish two viable device models: one with and the other without mirror symmetry across the center plane of the structure. Large tunnel magnetoresistance ratio (TMR) is predicted from first principles, at over 1800% and 3600% depending on the symmetry. Microscopically, a spin filtering effect is responsible for the large TMR. This effect essentially filters out all the minority spin channels (spin-down) from contributing to the tunnelling current. On the other hand, transport of the majority spin channel (spin-up) having Δ_1 and Δ_5 symmetry is enhanced by the FeO buffer layer in the MTJ. © *2015 AIP Publishing LLC*.
[http://dx.doi.org/10.1063/1.4929820]

I. INTRODUCTION

Since the discovery of tunnel magnetoresistance (TMR) phenomenon in Fe/Ge-oxide/Co sandwich structures,[1] the TMR effect has become the basic working principle of modern magnetic devices. In particular, magnetic tunneling junctions (MTJs) consisting of a thin insulating tunnel barrier sandwiched between two ferromagnetic contacts has been extensively investigated for applications in read sensors, magnetoresistive random access memory cells (MRAM), and programmable logic elements.[2,3] At present, the amorphous AlO_x (Ref. 4) and crystalline MgO (Ref. 5) are two commonly used insulators in MTJ. In particular, room temperature TMR values of 180%–600% in MgO-based MTJs were reported experimentally by several groups[6–8] and at low temperature, TMR greater than 1100% was achieved.[8]

For an ideal Fe/MgO/Fe MTJ, as explained before,[9,10] by symmetry the minority-spin *d*-states having transverse momentum $k_{||} \neq (0,0)$ in Fe, cannot couple to the slowly decaying Δ_1 band of MgO at the Γ-point $k_{||} = (0,0)$. These Fe states are thus filtered out by MgO. Furthermore, the majority-spin channel in one Fe cannot tunnel to the second Fe when magnetic moments of the two Fe are in anti-parallel configuration (APC). Overall, there is a very small APC current and a large spin polarized PC current, leading to very large TMR—as large as many thousands percent in the ideal limit as predicted by first principles calculations.[9,11] In comparison, the amorphous AlO_x barrier has no crystalline symmetry thus no coherent filtering effect, hence AlO_x based MTJ has much smaller TMR than MgO systems. In real devices, the inevitable interface disorder such as oxygen vacancy[12–14] in MgO significantly reduces TMR from the ideal limit.

For applications of MTJ in MRAM, it is critical to understand and mitigate the inevitable material imperfections. For MgO, the origin of these imperfections may be traced to the MgO-metal lattice mismatch and the fact that MgO is grown from two separate atomic sources (Mg and O). As pointed out in Ref. 15, the quality of such oxide films is lower than the insulating alkali halides such as NaCl and KBr films which are evaporated thermally to form predominantly molecular dimers. The growth of NaCl and KBr is much better controlled due to the reduced complexity of surface nucleation.[15] In principle, NaCl also has similar electronic properties as MgO.

A very interesting question therefore arises: Will alkali halide films make good MTJs? So far the answer appears to be positive theoretically[16] for the Fe/NaCl/Fe(001) MTJ but negative experimentally[17] for the same device. A reason may be due to strain between Fe and NaCl layers. To reduce strain, Ref. 18 theoretically investigated the FePt/NaCl interface and found the strain to be relatively small and spin injection from the FePt metal to the NaCl barrier is significant. Experimentally,[17] it turned out to be difficult to grow perfect NaCl films on Fe because NaCl corrodes metal surface and requires a high annealing temperature.

Recently, Tekiel *et al.*[15] reported an important experimental advance that successfully overcame the corrosion problem by introducing a buffer oxygen layer between the Fe substrate and the NaCl film, as a result perfect and large area NaCl films can be easily grown on the Fe(001) surface. It appears that the chemisorbed oxygen layer prevents the Fe surface from reacting to the NaCl overlayer. In addition, the higher chemical stability allows higher temperatures during growth which enhances NaCl diffusion and improves film quality. This important experimental advance[15] motivates us

[a)]Also at State Key Laboratory of Quantum Optics and Quantum Optics Devices, Institute of Laser Spectroscopy, Shanxi University, Taiyuan 030006, China. Electronic mail: zhanglei@physics.mcgill.ca.

to revisit the question concerning realization of MTJ devices based on alkali halides.

In particular, since NaCl films have grown perfectly and large area on the Fe (001)-p(1 × 1)O surface,[15] in this work we propose and theoretically investigate a novel MTJ, Fe(001)/O/NaCl(001)/O/Fe(001). Our first principles analysis shows that for this device, the TMR ratio can reach 3600% at low temperature. From the calculated scattering states, we conclude those with the Δ_1 and Δ_5 symmetry dominate the transmission of the majority spin channel through the NaCl barrier resulting to the large TMR. We also found that the device attains the highest TMR when the two Fe(001) contacts has mirror symmetry to each other. Microscopically, here in PC the majority spin channel traverses the NaCl barrier not around the Γ-point $k_{||} = (0, 0)$, but through very sharp transmission resonances or hot spots in the two dimensional (2D) Brillouin zone (BZ) away from the Γ-point. In fact, the entire tunneling process in both PC and APC for both majority and minority channels are dominated by the hot spots. Due to the experimental viability and easiness of the material growth,[15] the proposed Fe(001)/O/NaCl(001)/O/Fe(001) MTJ should be a very attractive system for practical applications.

The rest of the paper is organized as follows. In Sec. II, the device model and computational techniques are presented. Section III presents the transport properties of the Fe/O/NaCl/O/Fe MTJ, and Section IV provides further discussions and summary of the work.

II. DEVICE MODEL AND THEORETICAL METHOD

Before analyzing transport properties of the MTJ, we first establish the device model by calculating the structural properties of the contact interface between NaCl and Fe (001)-p(1 × 1)O. To this end, we relax the structure by density functional theory (DFT) with the projector augmented plane wave (PAW) method[19] and the local spin density approximation (LSDA) for the exchange-correlation functional,[20] using the VASP electronic package.[21] Semiempirical van der Waals (vdW) interaction is included[22,23] in the structure optimization. The Fe contact is adopted from the experimental structure[15] with lattice constant $a_0 = 2.86$ Å. Total energy calculation suggests that the NaCl unit cell is oriented at 45° with respect to Fe(001) substrate, leading to a 4 × 4 superstructure, in agreement with the experimental observations.[15,24] The epitaxial relationship between NaCl and Fe (001)-p(1 × 1)O substrate is presented in Figs. 1(a) and 1(b) where the (3 × 3) NaCl(001)[001] unit cells contact with (4 × 4) Fe(001)-O[110] unit cells in a 45° orientation. In this superstructure, the oxygen atoms are located at the hollow-site of the Fe(001) surface.[25]

Starting from the above superstructure suggested by total energy, a further structure relaxation is carried out for the supercell shown in Fig. 1(b). The supercell contains four layers Fe atoms, one layer of oxygen atoms absorbed on the Fe slab, three layers NaCl atoms, and a vacuum region of 15 Å thick. To make the relaxation feasible, the bottom three layers of Fe are fixed at their bulk positions while the topmost Fe, the oxygen, and NaCl atoms are allowed to relax until the residual force on each atom is smaller than

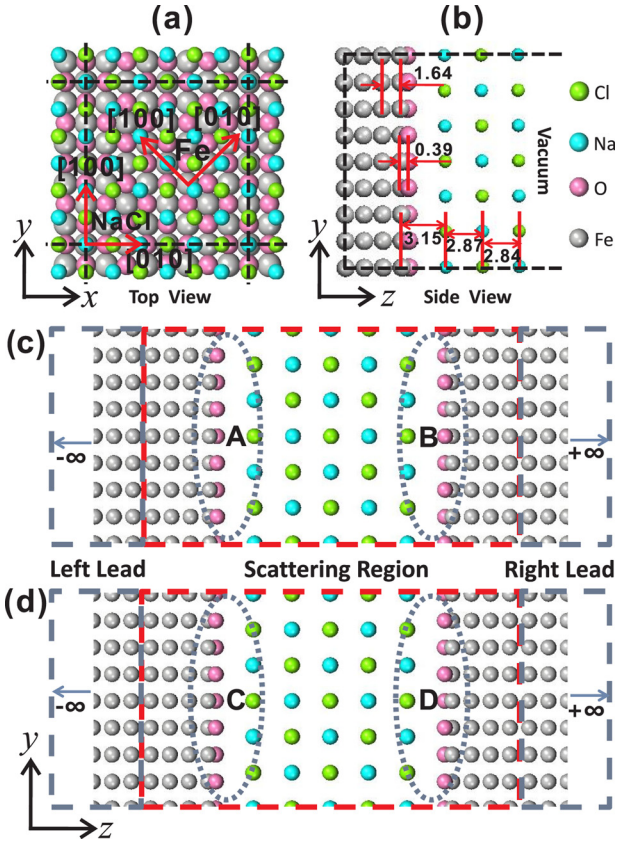

FIG. 1. (a) The top view of FeO and NaCl interfacial structure, and the epitaxial relationship is $Fe[110](001)||p(1 \times 1)O\ ||NaCl[001](001)$. (b) The side view of interfacial structure after relaxation. The unit of interface distance is Å and the black dashed line in (a) and (b) indicates the superstructure. (c) and (d) At the side views of the MTJs with the non-mirror symmetry (NMSS) and mirror symmetry (MSS) structures, respectively. The red dashed rectangles in (c) and (d) represent the scattering region in the transport analysis.

0.01 eV/Å along the z-direction. A k-mesh of 2 × 2 × 1 and energy cutoff 500 eV are used in the relaxation to ensure numerical accuracy. The distance marked in Fig. 1(b) is the final equilibrium separation along the z-direction between each adjacent layers after this structural relaxation. Note that the separation between the oxygen layer and the closest Fe layer in the z-direction is only 0.39 Å, indicating that an oxidized FeO layer forms at the surface of the Fe substrate. In addition, the distance between the NaCl slab and its closest Fe layer is 3.15 Å (as marked), at such a distance it is necessary—as we have done, to include the vdW interaction[22,23] during the relaxation.

Having determined the relaxed geometry of the NaCl/O/Fe interface, we build a two-terminal transport MTJ device as shown in Figs. 1(c) and 1(d). The two-terminal structure is naturally divided into three regions: the central scattering region and the left/right Fe electrodes. The MTJ is periodic in the *x*–*y* direction and the two Fe electrodes extend to $z = \pm\infty$ (transport direction). The central scattering region contains 500 atoms in total, including four layers of Fe atoms, one layer oxygen on both sides of NaCl, and five layers of NaCl as the tunnel barrier. For first principles quantum transport analysis, this is a very large system as dictated by the NaCl on Fe superstructure.

Since the unit cell of *bcc* Fe in the (001) direction contains two layers of Fe, two different MTJ structures are possible. The first is a non-mirror symmetry structure (NMSS), Fig. 1(c); and the second is a MSS, Fig. 1(d). For the NMSS device, the contacts between FeO and NaCl at both interfaces marked by A and B in Fig. 1(c) do not have mirror symmetry with respect to the NaCl barrier. For MSS, the contact interfaces marked C and D in Fig. 1(d) have mirror symmetry. According to our calculation, the total energy difference between these two device structures is extremely small, less than 1 meV/atom, indicating that both are experimentally possible. We have therefore investigated quantum transport properties of both device models.

Having determined the device model of the two-terminal MTJ, we perform first principles quantum transport analysis by carrying out DFT within the Keldysh nonequilibrium Green's function (NEGF) formalism,[26] as implemented in the first principles quantum transport package Nanodcal.[26–28] In our NEGF-DFT self-consistent calculations, a linear combination of atomic orbital basis (LCAO) at the double-ζ polarization (DZP) level is used to expand physical quantities; the standard norm-conserving nonlocal pseudo-potentials[29] are used to define the atomic core. The energy cutoff for the real space grid is taken at 100 Ry. To accurately determine quantum transport properties of the MTJ, a much denser 2D $k_\parallel$-mesh ($k_\parallel \equiv k_x, k_y$) is required, at 101×101. We refer interested readers to Refs. 26 and 27 for further details of the NEGF-DFT formalism and to Ref. 28 for details of the software.

After the NEGF-DFT self-consistent calculation of the device Hamiltonian is converged for the open two-terminal structure, the spin-polarized tunneling conductance is obtained by the Landauer formula

$$G^\sigma = \frac{e^2}{h}\sum_{k_\parallel} T_\sigma\left(k_\parallel, \epsilon\right), \tag{1}$$

here $\sigma \equiv \uparrow,\downarrow$ is the spin index, $T_\sigma(k_\parallel,\epsilon)$ is the spin dependent transmission coefficient at the energy ϵ with $k_\parallel = (k_x, k_y)$. $T_\sigma(k_\parallel,\epsilon)$ is calculated by the standard Green's functions approach.[26–28] Finally, the TMR ratio of the MTJ at zero bias voltage is obtained as

$$\mathrm{TMR} = \frac{G_{PC} - G_{APC}}{G_{APC}}, \tag{2}$$

where G_{PC} and G_{APC} are the conductances when the magnetization of the two Fe electrodes are in PC and APC, respectively.

III. TRANSPORT PROPERTIES

For the two possible MTJ structures, NMSS and MSS, we perform self-consistent NEGF-DFT calculations at both PC and APC. The results are summarized in Table I. For NMSS, the TMR ratio is 1800% and for MSS it is more than 2 times larger, 3600%. Either device model has impressive TMR values—comparable to that of the ideal MgO devices. By investigating the conductance of each spin channel, we found that the primary reason for the difference between NMSS and MSS is that the spin-up channel in PC ($G^\uparrow_{PC}$) of MSS is significantly larger than that of the corresponding value of NMSS. Namely, due to the mirror symmetry, it is easier to tunnel through MSS structure than to NMSS structure. Since $G^\uparrow_{PC}$ dominates the outcome, we obtain the 2 times larger TMR for MSS than NMSS devices.

TABLE I. The calculated conductance of each spin channel (in units of $10^{-5}\ e^2/h$) and TMR ratio for NMSS and MSS structures at the Fermi level. $G^\uparrow_{PC/APC}$ and $G^\downarrow_{PC/APC}$ represent spin-up (↑) and spin-down (↓) conductance in PC/APC, respectively.

Structure	$G^\uparrow_{PC}$	$G^\downarrow_{PC}$	$G^\uparrow_{APC}$	$G^\downarrow_{APC}$	TMR (%)
Non-mirror symmetry	9.11	4.02	0.331	0.334	1874
Mirror symmetry	69.3	3.37	0.976	0.975	3625

To understand why very large TMR values are possible in the Fe/O/NaCl/O/Fe MTJ, we investigated the microscopic tunneling process. The transmission coefficient resolved in the 2D BZ $k_\parallel \equiv (k_x, k_y)$ at the Fermi level, $T(\epsilon_F, k_\parallel)$, is plotted in Fig. 2 which provides a vivid physical picture of how tunneling is realized in this device. At a first glance, all patterns have a four-fold rotational symmetry, consistent with the C_{4v} symmetry of the MTJ superstructure. The MSS results [Figs. 2(a)–2(d)] and NMSS [Figs. 2(e)–2(h)] results have similar patterns but quite different values (see the side bar): the conductance of MSS is much larger than that of NMSS especially for PC configurations [comparing Figs. 2(a) and 2(b) with Figs. 2(e) and 2(f)], due to the structural mirror symmetry of the MSS model.

We note that hot spots—the very sharp transmission features in Fig. 2, dominate tunneling for all cases. This is very different from the MgO tunnel barrier[9,11] where for spin-up in PC, transmission is dominated by a broad peak at the Γ-point ($k_\parallel = 0$). Here, the lack of such a Γ-point broad peak indicates that the microscopic tunneling process is quite different from the Fe/MgO/Fe MTJ. For the Fe/O/NaCl/O/Fe, there is a significant magnetic moment of 0.23 μ_B per oxygen atom (parallel to the Fe magnetic moment), suggesting a very strong hybridization between the oxygen atoms and their neighboring Fe atoms. The strong hybridization dramatically reduces the density of states (DOS) contributed by the d_{z^2} orbital of Fe in the interfacial region, namely, it dramatically reduces the interface states having the Δ_1 symmetry near the Γ point in the Fe/O/NaCl/O/Fe MTJ.

The large TMR in the Fe/O/NaCl/O/Fe device is due to a spin dependent filtering effect, reminiscent to what happens in the MgO MTJ.[9,30–32] To reveal its microscopic origin, we now analyze the transmission hot spots. To be more specific but without losing generality, we pick a hot spot at $k_\parallel = (0.42, 0.30)$ (unit π/a_0) for MSS as an example [see red circles in Figs. 2(a) and 2(b)], results shown in Fig. 3. As discussed above, our system has a C_{4v} symmetry for which the slowest decaying Δ_1 band contains s, p_z, and d_{z^2} orbitals; the evanescent Δ_5 band contains d_{xz}, d_{yz}, p_x, and p_y orbitals; and finally, the Δ_2 and $\Delta_{2'}$ bands contributed by the $d_{x^2-y^2}$ and d_{xy} orbitals, respectively. By projecting the *density of scattering states* (DOSS)[33] into different orbitals and hence the

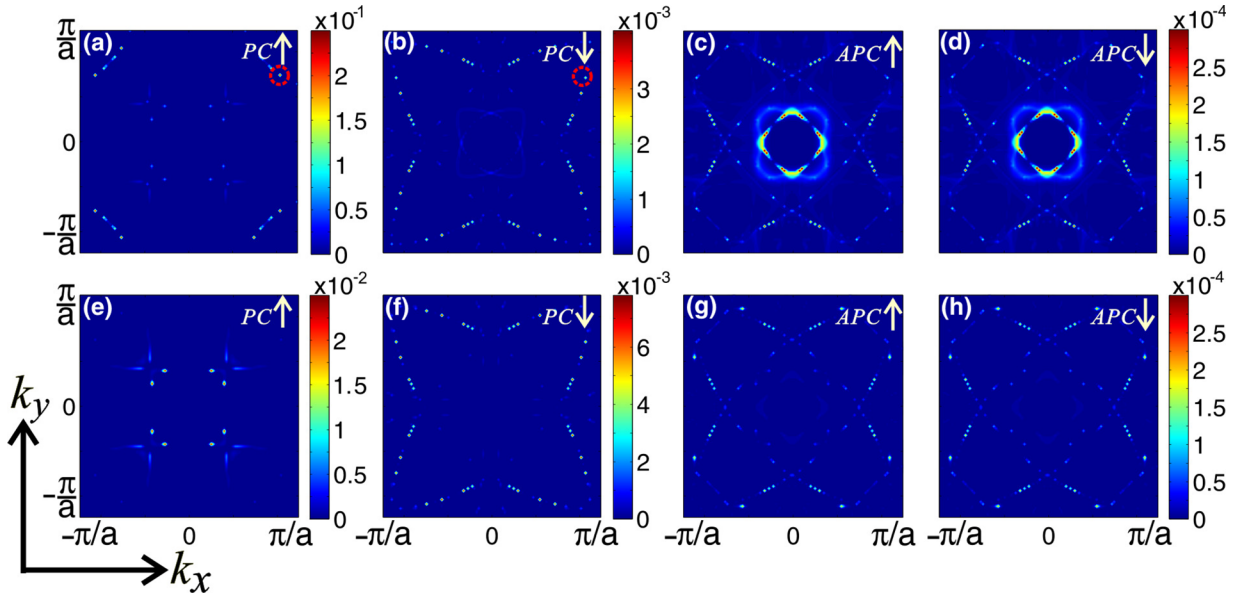

FIG. 2. Transmission hot spot or the $k_{\parallel} \equiv (k_x, k_y)$ resolved transmission coefficient $T = T(E_f, k_x, k_y)$ plotted in the 2D BZ for the spin-up and spin-down channels in PC and APC. (a)–(d) for MSS MTJ; (e)–(h) for NMSS MTJ. (a) and (e) for spin-up and (b) and (f) for spin-down in PC; (c) and (g) for spin-up and (d) and (h) for spin-down in APC. The results are shown on a 101×101 $k_{\parallel}$-mesh at the Fermi level of the MTJ. The $k_{\parallel} = (0.42, 0.30)\frac{\pi}{a_0}$ point is marked by red circles in (a) and (b).

different symmetry components (e.g., the Δ bands), the contribution from each symmetry components is revealed. Note that a scattering state is an eigenstate of the two-terminal device Hamiltonian that extends from the left electrode to the right electrode through the scattering region. DOSS measures the number of scattering states in unit energy for transport and it plays a similar role as the DOS in electronic structure analysis. As shown in Figs. 3(a) and 3(b), we found that DOSS of both spin channels with Δ_5, Δ_2, and $\Delta_{2'}$ symmetry decay quickly near the Fe/O/NaCl interface. On the other hand, DOSS for those having the Δ_1 symmetry decay two orders of magnitude slower, hence Δ_1 dominates tunneling for both spin channels. As shown in Fig. 3(a), the Δ_1 symmetry states decay by two orders of magnitude at the Fe layer nearest to the oxygen (the forth Fe layer, horizontal axis) due to formation of FeO which significantly prevents the d_{z^2} orbitals of Fe from contributing to transport. A similar situation occurs in MgO devices as reported in Ref. 32 when there is a FeO layer. Importantly, the main contribution of Δ_1 symmetry states in the NaCl barrier comes from s and p_z orbitals. Note that scattering states with Δ_2 and $\Delta_{2'}$ symmetry composed by orbitals in the x-y plane do not couple to the $p-$ orbitals of oxygen, as a result DOSS coming from these two symmetry states decay immediately at the fifth layer when they go through the oxygen region (see Fig. 3).

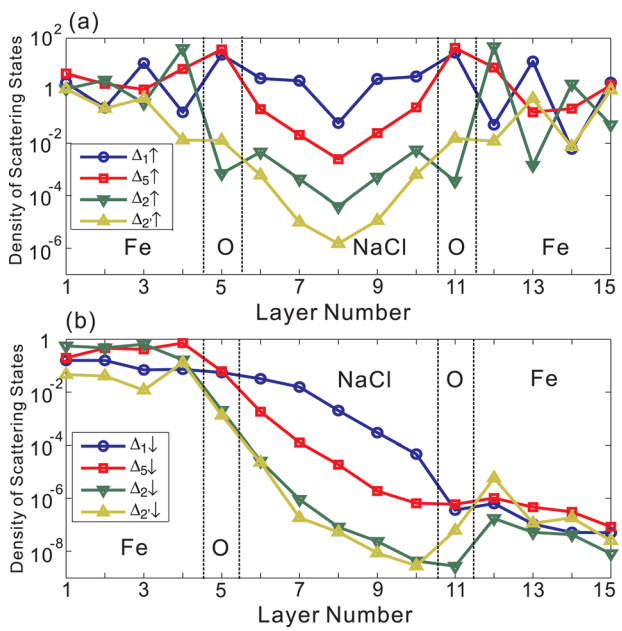

FIG. 3. Density of Scattering States (DOSS) (Δ_1, Δ_5, Δ_2, $\Delta_{2'}$) on each atoms layer at $k_{\parallel} = (0.42, 0.30)\frac{\pi}{a_0}$ point for MSS MTJ. (a) For spin-up channel in PC; (b) for spin-down channel in PC. The location of Fe, O, and NaCl layers has been marked.

Very interestingly, for the spin-up channel and due to the formation of interfacial resonant states[34] in the FeO layer, DOSS with Δ_1 and Δ_5 symmetries significantly enhance in the oxygen layers (blue and red curves at the 5-th and 11-th layer), as shown in Fig. 3(a). The spin-down channel at the same $k_{\parallel} = (0.42, 0.30)$(unit π/a_0) is however not a transmission hot spot (see Fig. 2(b)) which means the corresponding scattering state should not be interfacial resonant state in the FeO layer. Indeed, the corresponding DOSS in Fig. 3(b) confirms that there is no enhancement at the oxygen layer. Comparing with the spin-up channel, the DOSS of the outgoing spin-down scattering states in the right Fe lead are five orders of magnitude smaller. We conclude that there is a strong spin dependent filtering effect by the FeO/NaCl barrier region that filters out spin-down channels. In APC, the current is contributed by incoming electronics in the spin-up channel but outgoing in the spin-down channel (and vice versa), the filtering reduces APC current very effectively (see Fig. 4 below) resulting to a large TMR by Eq. (2).

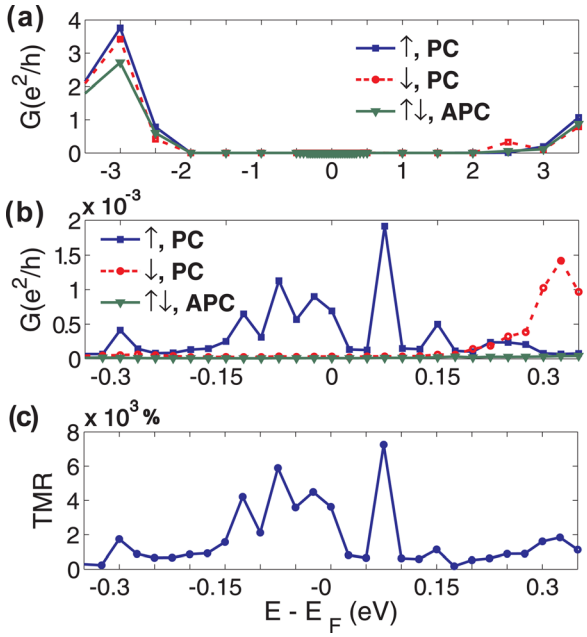

FIG. 4. (a) The conductance at energies between −3.5 and 3.5 eV. Square solid line: $G^{\uparrow}$ for PC; dotted dashed line: $G^{\downarrow}$ for PC; inverted triangle solid line: $G^{\uparrow} = G^{\downarrow}$ for APC. $E = 0$ is the Fermi level of leads. (b) Zoom in conductance G^{σ} versus energy E for MS MTJ. (c) The TMR ratio versus energy E[−0.35 eV, 0.35 eV] for MSS MTJ.

Fig. 4 plots the calculated spin-polarized conductance G^{σ} and TMR versus incoming electron energy E, for the MSS device. Fig. 4(a,b) shows G^{σ} for PC and APC. In PC, $G^{\uparrow}$ is several orders of magnitude larger than $G^{\downarrow}$ near the Fermi level ($-0.1 < E < +0.1$ eV). In APC, $G^{\uparrow} = G^{\downarrow}$ due to the geometrical symmetry of the device structure, and both have tiny values (solid triangular line). Quantitatively, the spin filtering effect essentially removed the spin-down channel in PC and both channels in APC from the tunneling process, resulting to huge TMR values as shown in Fig. 44(c). Even though TMR at Fermi energy (shifted to $E = 0$) is 3625%, it reaches over 6000% slightly below E_f as shown by the large peak in Fig. 4(c). Finally, we note that while TMR is large, the tunnel conductance itself is small (Fig. 4(b)). The inset of Fig. 4(c) plots the tunnel conductance versus energy for a much wider energy range $-2.0 < E < 2.0$ eV, which clearly shows the tunnel gap due to the NaCl insulator (the calculated LSDA bulk gap of NaCl is 4.7 eV). Here, large conductance results from transport in the valence bands at $E < -2$ eV, thus the small tunneling conductance inside the gap cannot be discerned in the figure.

IV. DISCUSSION AND SUMMARY

Motivated by the experimental growth of perfect and large area Fe/O/NaCl interface structures,[15] we have proposed a novel MTJ device with the Fe/O/NaCl/O/Fe sandwich structure. We establish the device model by total energy relaxation and found that NaCl is oriented at 45° with respect to Fe(001) substrate leading to a 4×4 superstructure consistent with the experimental observation.[15] Total energy relaxation also revealed that oxygen atoms at the interface form a Fe(001)-p(1×1)O structure by locating at the hollow-sites of the Fe(001) surface. With the help of the oxygen atoms, there exists extremely small strain (after relaxation) between the Fe 4×4 superstructure and the NaCl 3×3 barrier layer, consistent with the experimental indications.[15]

The resulting Fe/O/NaCl/O/Fe device model is analyzed by first principles quantum transport theory. The TMR ratio of NMSS can reach over 1800%, while more interestingly for the MSS it reaches 3600% at the Fermi level. By investigating scattering states, we find that the s and p_z orbitals with Δ_1 symmetry dominate the tunneling conductance. The d_{z^2} orbitals with Δ_1 symmetry decay rapidly due to the FeO layer at the junction interface, resulting to very small transmission coefficient around the Γ-point. At the same time, the presence of interface resonant states (hot spots) leads to a significant enhancement of transport—as measured by the DOSS, with Δ_1 and Δ_5 symmetries at the FeO layer. Due to these symmetries, a significant spin filtering effect is at work which essentially removes transmission of spin-down channels and, in the end, only the spin-up channel in PC has significant contribution to tunneling, resulting to the large TMR ratio. These results strongly suggest that the proposed Fe/O/NaCl/O/Fe device may well be an attractive MTJ from both fabrication and TMR point of views.

Finally, we note that a *crystal* of FeO has a strong electronic correlation and should be analyzed by methods such as LDA + U.[35] The question is if a *layer* of FeO (as in our device) gives special correlation effects to qualitatively alter the above conclusions. To this end, we note that Timoshevskii *et al.*[31] have systemically analyzed the influence of transport properties of Fe/FeO/MgO MTJs by taking into account the on-site Coulomb repulsion in the FeO layer. They found that the correlation effects in that FeO layer cause a collapse of Fe d_{z^2} and $d_{x^2-y^2}$ states at the Fermi level, namely, the correlations in FeO layer suppress transport with Δ_1 symmetry near the Γ-point ($k_{\|} = 0$). This may be important for MgO but not for NaCl, because in the Fe/O/NaCl/O/Fe MTJ, it is the s and p_z orbitals at the FeO/NaCl interface that dominate tunneling for both spin channels and there is essentially no Γ-point transmission. Hence, such correlation effect, if exists, will not alter the qualitative conclusion that very large TMR can be realized by the Fe/O/NaCl/O/Fe device.

ACKNOWLEDGMENTS

We thank Dr. Dongping Liu for his participation at early stages of this work. This work was supported by NSERC of Canada (H.G.) and the China Scholarship Council (K.G.). We thank CLUMEQ, CalcuQuebec, and Compute-Canada for providing computation facilities.

[1]M. Julliere, Phys. Lett. A **54**, 225 (1975).
[2]M. Tondra, J. M. Daughton, D. Wang, R. S. Beech, A. Fink, and J. A. Taylor, J. Appl. Phys. **83**, 6688 (1998).
[3]M. Durlam *et al.*, IEEE J. Solid-State Circuits **38**, 769 (2003).
[4]X. Han *et al.*, Jpn. J. Appl. Phys., Part 2 **39**, L439 (2000).
[5]S. Yuasa and D. D. Djayaprawira, J. Phys. D: Appl. Phys. **40**, R337 (2007).
[6]S. Yuasa, T. Nagahama, A. Fukushima, Y. Suzuki, and K. Ando, Nat. Mater. **3**, 868 (2004).

[7]S. Parkin, C. Kaiser, A. Panchula, P. Rice, B. Hughes, M. Samant, and S. H. Yang, Nat. Mater. **3**, 862 (2004).
[8]S. Ikeda, J. Hayakawa, Y. Ashizawa, Y. Lee, K. Miura, H. Hasegawa, M. Tsunoda, F. Matsukura, and H. Ohno, Appl. Phys. Lett. **93**, 082508 (2008).
[9]W. H. Butler, X.-G. Zhang, T. C. Schulthess, and J. M. MacLaren, Phys. Rev. B **63**, 054416 (2001).
[10]J. Mathon and A. Umerski, Phys. Rev. B **63**, 220403 (2001); **71**, 220402(R) (2005).
[11]D. Waldron, V. Timoshevskii, Y. Hu, K. Xia, and H. Guo, Phys. Rev. Lett. **97**, 226802 (2006).
[12]P. G. Mather, J. C. Read, and R. A. Buhrman, Phys. Rev. B **73**, 205412 (2006).
[13]G. X. Miao *et al.*, Phys. Rev. Lett. **100**, 246803 (2008).
[14]Y. Ke, X. Ke, and H. Guo, Phys. Rev. Lett. **105**, 236801 (2010).
[15]A. Tekiel, J. Topple, Y. Miyahara, and P. Grütter, Nanotechnology **23**, 505602 (2012).
[16]P. Vlaic, J. Magn. Magn. Mater. **322**, 1438 (2010).
[17]M. Nakazumi, D. Yoshioka, H. Yanagihara, E. Kita, and T. Koyano, Jpn. J. Appl. Phys., Part 1 **46**, 6618 (2007).
[18]L. L. Tao, D. P. Liu, S. H. Liang, X. F. Han, and H. Guo, Europhys. Lett. **105**, 58003 (2014).
[19]P. E. Blochl, Phys. Rev. B **50**, 17953 (1994).
[20]J. P. Perdew and Y. Wang, Phys. Rev. B **45**, 13244 (1992).
[21]G. Kresse and J. Hafner, Phys. Rev. B **47**, 558 (1993).
[22]S. J. Grimme, Comput. Chem. **27**, 1787 (2006).
[23]T. Bučko, J. Hafner, S. Lebègue, and J. G. Ángyán, J. Phys. Chem. A **114**, 11814 (2010).
[24]In this superstructure, the lattice mismatch is about 4.1%. In the numerical simulation, the NaCl lattice is suppressed to march with Fe cell.
[25]P. Błoński, A. Kiejna, and J. Hafner, Surf. Sci. **590**, 88–100 (2005).
[26]J. Taylor, H. Guo, and J. Wang, Phys. Rev. B **63**, 245407 (2001).
[27]D. Waldron, P. Haney, B. Larade, A. MacDonald, and H. Guo, Phys. Rev. Lett. **96**, 166804 (2006).
[28]See http://www.nanoacademic.ca for details of the NanoDcal quantum transport package.
[29]L. Kleinman and D. M. Bylander, Phys. Rev. Lett. **48**, 1425 (1982).
[30]W. H. Butler, Sci. Technol. Adv. Mater. **9**, 014106 (2008).
[31]V. Timoshevskii, Y. Hu, É. Marcotte, and H. Guo, J. Phys.: Condens. Matter **26**, 015002 (2014).
[32]X. G. Zhang, W. H. Butler, and A. Bandyopadhyay, Phys. Rev. B **68**, 092402 (2003).
[33]Here, the orbital dependent DOSS is calculated by $DOSS(\mu) = \sum_\alpha c^*_{\alpha\mu} c_{\alpha\mu}$, where $c_{\alpha\mu}$ is the coefficient of corresponding αth scattering wave function in orbital space, i.e., $\psi_\alpha(\mathbf{r}) = \sum_\mu c_{\alpha\mu}\phi_\mu(\mathbf{r})$; $\phi_\mu(\mathbf{r})$ is the atomic orbital.
[34]O. Wunnicke, N. Papanikolaou, R. Zeller, P. H. Dederichs, V. Drchal, and J. Kudrnovsky, Phys. Rev. B **65**, 064425 (2002).
[35]V. I. Anisimov and O. Gunnarsson, Phys. Rev. B **43**, 7570 (1991).